Effect of pulsing parameters on laser ablative cleaning of copper oxides

Jie Zhang,[a] Youneng Wang, Peng Cheng, and Y. Lawrence Yao
Department of Mechanical Engineering, Columbia University, 220 Mudd Building, MC 4703, New York, New York 10027

(Received 29 June 2005; accepted 23 January 2006)

The characteristics of copper oxide removal are comparably investigated under different pulsing strategies. A two-dimensional model is utilized to numerically simulate the laser ablative cleaning process. In the model, property discontinuity and Stephan and kinetic boundary conditions are taken into account, and the moving phase interface in the material is evaluated with the enthalpy method. Experiments are carried out on copper samples having different oxide layer thicknesses. The copper oxide layer thicknesses determined by ellipsometer and the chemical constituents of the copper oxide layer determined via x-ray photoelectron spectroscopy are incorporated into this numerical model. Under the single-pulse irradiation strategy, a higher laser intensity threshold is determined by the model based on the criterion of removing the oxide film as much as possible without damaging the substrate. Under the multipulse irradiation strategy, a lower threshold is employed to remove the oxide layer, while the appropriate pulse numbers under different laser intensities and different laser pulse repetition rates are the key issues investigated. A reasonable agreement is obtained between the experimental and simulated results. © *2006 American Institute of Physics*.
[DOI: 10.1063/1.2175467]

I. INTRODUCTION

How to remove contaminations and oxides from surfaces has been an active research topic for many years in that clean surfaces are extremely vital in the fabrication of semiconductors,[1] microelectronic devices and integrated circuits, and even in the maintenance of a nuclear reactor.[2] At present, the wet chemical flux and ultrasonic/megasonic are the most widely used methods to clean surfaces. However, the former is not environmentally benign, and the latter cannot produce sufficient cleaning forces in some cases. The disadvantages of these methods stimulated researchers to seek alternative cleaning methods.

Laser cleaning using short pulsed laser irradiation to clean surfaces has emerged as a promising method because of its prominent advantages such as selectivity, controllability, and flexibility. Moreover, laser cleaning is easy to be automated and integrated into the production line. Besides being explored for use in art restoration, this environment-friendly technique is also utilized to remove nanoscale particles from semiconductor surfaces,[3] to strip painting or oxide layers from metals or semiconductors.[4–6] Furthermore, laser cleaning can be integrated into other cleaning methods to significantly enhance the cleaning efficiency.[7]

Laser removal of a thin contamination layer from the substrate mainly involves several competing mechanisms, such as ablation, photospallation, and acoustic excitation due to rapid thermal expansion.[8] For the transparent layer, such as silicon dioxide, the acoustic pulse induced by the absorption of the laser energy at the substrate/layer interface is the main power to remove the thin layer.[9] For the opaque layer, if the applied laser intensity is too low to melt the layer, the thermal stress due to the very rapid heating of laser pulse is responsible for the layer removal.[10] Generally, the relatively high laser intensity is used to remove the contamination layer based on the working mechanism of laser ablation.

Copper is the most widely utilized metal in the fabrication of printed circuit boards and integrated circuits due to its excellent electrical conductivity and less electromigration. However, the disadvantages of Cu are that it is easy to be naturally oxidized and its oxidation is not self-limiting, which imposes a significantly negative effect on the work performance of the entire system. Therefore, the laser removal of copper oxide dominated by the ablation mechanism has drawn the investigation interests.

Wesner *et al.* explored the possibility of the laser removal of copper oxide and monitored the cleaning results with x-ray photoelectron spectroscopy (XPS) spectrum analysis.[11] Yonezawa *et al.* found that the results of the copper oxide removal were dependent on the applied laser intensity. And the morphology change was possibly due to the explosion or transport of molten materials.[12] Kearns *et al.* investigated the effect of wavelength on the laser fluence threshold for the laser removal of copper oxide as well as the material removal mechanisms at different laser wavelengths.[13]

Pulse parameters play a key role in the success of the laser cleaning, namely, removing the contaminations or oxides without any damage to the underlying substrate. Wesner *et al.* found that a large number of pulses at a low fluence could achieve the cleaning quality similar to that produced by a small number of pulses at a high fluence. And the thermal accumulation might limit the number of pulses and the fluence.[11] However, this area is far from fully understood, especially in the analytical sense. Lee *et al.* proposed a one-dimensional heat conduction model to numerically determine the laser fluence threshold for the cleaning of copper oxide and investigate the cleaning mechanism at different wave-

[a]Electronic mail: jz2112@columbia.edu

lengths based on this model.[14] However, this model was inaccurate due to the neglect of many basic phenomena of laser ablation. Lee *et al.* formulated a one-dimensional heat flow model incorporating melting and vaporization to seek the optimal processing conditions.[15] In this model, the property discontinuity at the Knudsen layer and the kinetic phase boundary were not considered.

In this paper, a two-dimensional mathematical model is utilized to more accurately simulate laser cleaning under the ablation mechanism. Under the single-pulse strategy, the laser intensity threshold is determined by experiments and simulations. Under the multipulse strategy, a lower threshold is employed to remove the oxide layer. The influence of laser intensity and repetition rate on pulse number is studied via experiments and numerical simulations.

II. EXPERIMENTAL CONDITIONS AND MEASUREMENTS

A. Experimental conditions

Laser irradiation experiments are performed using a *Q*-switched Nd:YAG (yttrium aluminum garnet) laser with a wavelength of 355 nm and a pulse duration of 50 ns. The laser beam intensity has a Gaussian distribution. The laser intensity irradiated on the sample surface can be adjusted through changing the distance between the sample and the focusing lens. Repetition rates of 1 and 2 kHz are used; the beam quality parameter M^2 is 1.49 and the minimal beam diameter is 12 μm.

The laser system is composed of the Nd:YAG laser source, charge-coupled device (CCD) camera, TV monitor, sample stages, and control system. The laser cleaning experiments are carried out in open air. During the experiments, a gas jet flows onto the sample to prevent the plasma formed by laser ablation from getting onto the focusing lens.

The samples are pure copper (15×15 mm^2, 0.8 mm thick), which are mechanically polished. They are divided into two groups and baked in an oven at 250 °C for 30 and 45 min, respectively. After baking, the copper oxide layers with two different thicknesses are formed to allow the study of the effect of oxide layer thickness on laser intensity threshold.

B. Material characterization

The thickness of the copper oxide layer is measured with the Beaglehole Spectroscopic ellipsometer. The ellipsometer is based on the measurement of the change in the state of light polarization caused by its interaction with the sample, defined with quantities Δ and ψ, to characterize thin films.[16] Film thicknesses and optical constants can be deduced from Δ and ψ using a model of optical physics. In this paper, ellipsometry measurements are performed at the Brewster angle of 68°. The wavelength of the incident light varies from 300 to 800 nm with a step of 4 nm. The software of FILMWIZARD is employed to deduce the results.

XPS (PHI 550 ESCA XPS ion scattering spectroscopy (ISS) spectrometer) is used to analyze the chemical constituents of pre- and postcleaned copper oxide layers. XPS uses soft x-ray sources (Al Kα and Mg Kα) to ionize electrons from the surface of a solid sample. The binding energies of these electrons are measured and are characteristic of the elements and the associated chemical bonds (chemical state) in the top few atomic layers of the material.[17] Usually, the measurement depth of XPS is around 10–30 nm.

The mechanism of the space-charge oxidation processes is helpful in verifing that the copper oxides formed at 250 °C are composed of cupric oxide (CuO) and cuprous oxide (Cu_2O) and their distributions vary along the thickness direction.[18] Due to the large electron affinity of the chemisorbed oxygen, electrons are withdrawn from the oxide to form ions (e.g., O^-) and additional holes are created in a *p*-type conducting oxide of Cu_2O, which results in the cation concentration being higher than the vacancy concentration. Hence, the space-charge field is set up, counteracting the chemical concentration gradient. The chemisorption of oxygen on the interface of the oxide is written as

$$\tfrac{1}{2}O_2^{(g)} + 2 \otimes (\mathrm{Cu}) \leftrightarrow Cu_2O + 2\mathrm{Cu} \oplus . \quad (1)$$

When the space-charge field is in equilibrium with the chemical concentration gradient, the growth of the oxide layer will cease. Before that, with the thickening of the oxide layer, more and more free electrons are thermally emitted and enter the space-charge layer. Rapid field transport of copper ions through vacancies keeps the stationary surface concentration of the oxygen low. Then, CuO is generated starting from the interface of oxygen and Cu_2O. A thin layer of Cu_2O always exists on the copper substrate.

Images of pre- and postcleaned copper oxide layers are obtained using scanning electron microscopy (JEOL JSM 5600). Atomic force microscopy (AFM) (Dimension 3000) is employed to measure the crater generated by the laser irradiation on the sample.

III. TWO-DIMENSIONAL LASER ABLATIVE CLEANING MODEL

During the laser ablative cleaning, the copper oxides are irradiated by the short laser pulse with extremely high intensity, and thus experience fast melting and intensive evaporation. The traditionally used heat conduction model has no capability of reflecting this complex laser-solid interaction process. In addition, the laser beam diameter used for the experiment in this paper is 20–100 μm. Although it is larger than the oxide thickness, which usually is a few microns, and the thermal diffusion distance $d=2\sqrt{\alpha\tau}=2.03$ μm, where α is thermal diffusivity of the copper oxides and τ is the pulse width of 50 ns in this case, it is desirable to use a two-dimensional model to analyze the thermal field in the material more realistically.

Zhang *et al.* developed a two-dimensional model to describe the laser ablation of copper.[19] In fact, laser ablative cleaning is based on the ablation of the oxide layer without damaging the substrate. However, this model of laser ablation cannot be directly used to delineate the ablative cleaning without the necessary modifications.

The laser ablative cleaning model developed in this paper assumes that the target has a two-layer structure, including copper oxides and copper, shown in Fig. 1. As mentioned

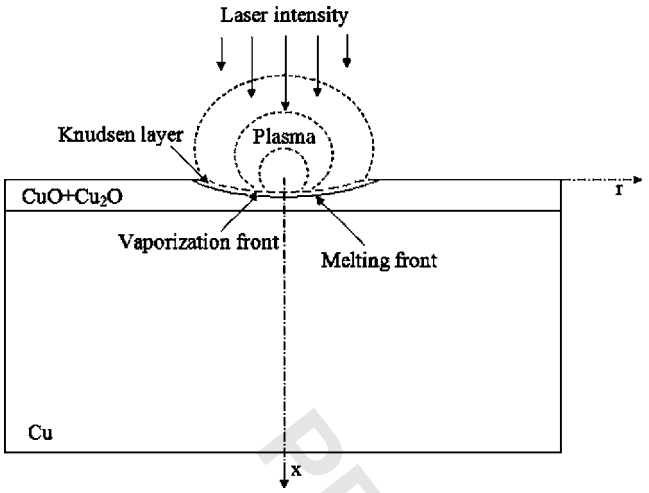

FIG. 1. Schematic of the two-dimensional laser ablative cleaning model.

before, the thickness of the copper oxide layer is determined using ellipsometry. Along the thickness direction, the distribution of CuO and Cu_2O is determined through the XPS spectrum analysis of the copper sample gradually etched away. Within the range of copper oxides and copper, the corresponding material properties are used.[20,21]

The laser intensity absorbed by the sample is $Q=C(1-\mathrm{Rl})Ie^{-(r/b)^2}$, where b is the laser beam radius. C is the plasma correction coefficient, which is the ratio of the reduced laser intensity due to the plasma absorption to the incident laser intensity. C is equal to 1 in the case of the incident intensity less than the threshold for plasma formation of 3×10^7 W/cm^2. When the incident intensity is larger than 3×10^7 W/cm^2, C is estimated as $C=0.629\,27-0.5\tanh[I-2.4(3\times10^8-3\times10^7)]/[2.4(3\times10^8-3\times10^7)]$, where the intensity of 3×10^8 W/cm^2 is called the threshold for strong plasma formation. These two intensity thresholds are determined by the crater-shape fit between the model and the experiments, respectively. I is the incident laser intensity.[22] The sample surface is well polished before the thermal oxidation. In addition, the depth of the ablation-formed crater is much smaller than its diameter; the crater is approximately viewed as a flat surface during the laser irradiation. Thus, the reflectivity Rl is calculated as $\mathrm{Rl}=[(n-1)^2+k^2]/[(n+1)^2+k^2]$, where n and k are the indices of refraction and extinction coefficient, respectively. At the wavelength of 355 nm, Cu has the index of refraction of 1.34, CuO has 2.24, and Cu_2O has 2.4. The extinction coefficient of Cu is 1.93, that of CuO is 1.03, and that of Cu_2O is 1.44.[23]

The model is briefly summarized as follows. It is assumed that the movement of the molten material and the heat loss from the surface are negligible. The heat conduction in the solid is described as

$$\frac{1}{\rho_0 c_p}\left[K\frac{\partial^2 T}{\partial x^2}+\frac{1}{r}\frac{\partial}{\partial r}\left(Kr\frac{\partial T}{\partial r}\right)\right]=\frac{\partial T}{\partial t}, \tag{2}$$

where t is the time, x and r are the coordinates along the thickness and radial directions, respectively, ρ_0 is the density of solid, c_p is the specific heat, and K is the heat conductivity.

At the vapor-liquid interface, the Stephan boundary condition is considered as[24]

$$Q+K\left(\frac{\partial T}{\partial x}+\frac{\partial T}{\partial r}\right)+\rho_l\nu_i L_\nu-\rho_\nu\nu_\nu(c_pT_i+E_\nu)=0, \tag{3}$$

where the gas energy $E_\nu=RT_\nu/(\gamma-1)M_\nu+\frac{1}{2}\nu_\nu^2$ includes the internal and kinetic energies. The subscripts l, ν, and i denote the liquid phase, vapor phase, and vapor-liquid interface, respectively. R is the universal gas constant, ν is the velocity, L_ν is the latent heat of vaporization, M_ν is the molecular mass, and γ is the specific heat ratio.

The property discontinuity across the Knudsen layer is described as[25]

$$\frac{T_{\nu i}}{T_{li}}=\left[\sqrt{1+\pi\left(\frac{m}{2}\frac{\gamma-1}{\gamma+1}\right)^2}-\sqrt{\pi}\frac{m}{2}\frac{\gamma-1}{\gamma+1}\right]^2,$$

$$\frac{\rho_{\nu i}}{\rho_{li}}=\sqrt{\frac{T_{li}}{T_{\nu i}}}\left[\left(m^2+\frac{1}{2}\right)e^{m^2}\,\mathrm{erfc}(m)-\frac{m}{\sqrt{\pi}}\right]+\frac{1}{2}\frac{T_{li}}{T_{\nu i}}[1-\sqrt{\pi}me^{m^2}\,\mathrm{erfc}(m)].$$

$$e^{m^2}\,\mathrm{erfc}(m)\approx 0.348\,02a-0.095\,88a^2+0.747\,86a^3, \tag{4}$$

where

$$a=1/(1+0.474\,07m),\quad m=\frac{V_{\nu i}}{\sqrt{2RT_{\nu i}/Ma_\nu}},$$

where νi and li denote the value of the vapor and liquid adjacent to the Knudsen layer, respectively. Ma_ν is the vapor Mach number, and $\mathrm{erfc}(m)$ the complementary error function. The gas velocity is obtained from mass conservation, such as $\rho_l\nu_i=\rho_\nu(\nu_i+\nu_\nu)$. Then, the vapor temperature calculated through Eq. (4) is inserted into the Stephan boundary condition [Eq. (3)]. The enthalpy method is applied to trace the interface of solid and liquid phases.[26] The above coupled equations are discretized into the implicit form through the control-volume method. Then, these algebraic discretization equations are solved through an iterative method called the tridiagonal matrix algorithm (TDMA) line-by-line method.[27] During a time step of 10 ns, the temperature is convergent as the relative error is less than 10^{-5}. According to the node temperature, the different phases of the materials are determined. The nodes within the vapor phase are excluded from the calculation of the next time step. The computation domain is chosen as five times the beam radius b in both x and r directions. Thus, the temperature at lines $x=5b$ and $r=5b$ is considered as room temperature, and line $r=0$ is viewed as the line of symmetry. The grids are divided with the bias method in both x and r directions. The finer the grids, the closer the grids to the beam center. All numerical calculations are realized with MATLAB.

In this paper, the evaporation temperatures of CuO, Cu_2O, and Cu are 2073, 2073, and 2833 K, respectively. The melting temperatures of CuO, Cu_2O, and Cu are 1609, 1515, and 1356 K, respectively.[20,21]

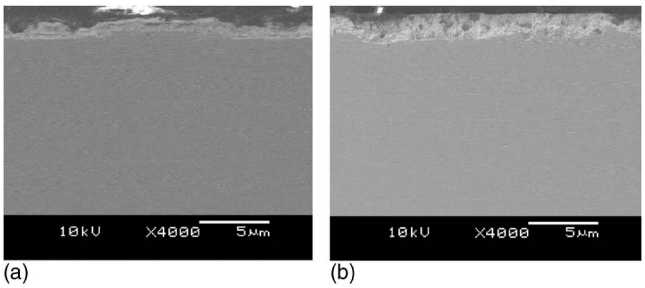

FIG. 2. SEM images of the cross section of the Cu samples with copper oxide layers: (a) sample 1 (oxidized at 250 °C for 30 min) and (b) sample 2 (oxidized at 250 °C for 45 min).

IV. RESULTS AND DISCUSSIONS

A. Copper oxide layer characterization

Figure 2 shows scanning electron microscopy (SEM) images of cross sections of two samples. It can be observed that the sample oxidized for 45 min has a thicker oxide layer than that of the sample oxidized for 30 min. This phenomenon is consistent with the conclusion that the oxide layer thickness increases with the oxidation temperature and time, following the parabolic rate law.[18] The thickness of the oxide layer is also measured with the ellipsometer. The measured and fitted Δ and ψ for these two samples are presented in Fig. 3. The root-mean-square errors between measured and fitted Δ and ψ of 6.28 in Fig. 3(a) and 3.79 in Fig. 3(b) show that the evaluated oxide layer thickness is relatively accurate. The oxide layer thickness is about 1 and 2.5 μm for the samples oxidized for 30 and 45 min, respectively.

The chemical distribution of copper oxides along the thickness direction is investigated with the XPS analysis. These two samples having different oxide layer thicknesses are etched by 9% hydrogen chloride for 2 s in the 1 μm case and 5 s in the 2.5 μm case, respectively. In both cases, the time increment is 1 s. The oxide layer thickness of the etched sample is assumed to be inversely proportional to the etching time.

The Cu 2*p* and O 1*s* XPS spectra of etched samples having 1 and 2.5 μm thick oxide layers are presented in Figs. 4(a) and 4(b), respectively. The binding energies of Cu 2*p* and O 1*s* associated with CuO and Cu_2O are listed in Table I. In Fig. 4(a), the spectrum after etching for 1 s displays a Cu $2p_{3/2}$ peak at 934.5 eV corresponding to CuO, a shake-up satellite peak at about 9 eV higher than the $2p_{3/2}$ peak, and a peak above 950 eV arising from spin-orbit coupling.[28] This shows that only CuO exists on the surface after 1 s etching. In the spectrum after etching for 2 s, the Cu $2p_{3/2}$ peak is located at 932.4 eV, which corresponds to Cu or Cu_2O. However, Cu_2O is ruled out based on two facts: no Cu 2*p* satellite peak is associated with Cu_2O, and the O 1*s* peak at 531 eV without any shift is caused by Cu_2O. This means that there are no copper oxides on the surface after 2 s etching. In Fig. 4(b), the spectra after etching for 1 and 2 s show that CuO still exists after 1 and 2 s etching. In the spectra after 3 and 4 s, the Cu $2p_{3/2}$ peak is located at 932.4 eV again. However, the satellite peak associated with Cu_2O at 946.5 eV denotes the appearance of Cu_2O. It can be verified with the O 1*s* spectrum. The O 1*s* peak shifts about

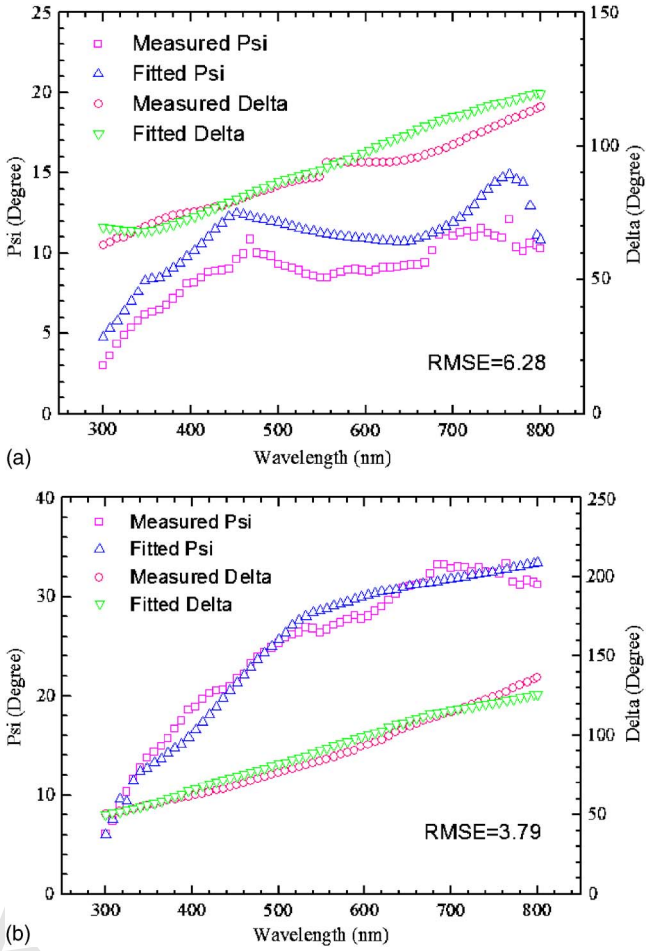

FIG. 3. (Color online) Comparison of measured and model fitted optical data in the ellipsometer measurement of the oxide layer thickness: (a) sample 1 (oxidized at 250 °C for 30 min) and (b) sample 2 (oxidized at 250 °C for 45 min).

0.7 eV to a lower binding energy mainly due to the presence of Cu_2O. The last spectrum (after etching for 5 s) shows no existence of copper oxides.

Suppose that the etching rates of CuO and Cu_2O with HCl are identical. According to the XPS analysis of the etched copper oxide layer, it can be deduced that the CuO layer is above the Cu_2O layer. For simplicity without losing generality, it is assumed that the top half of the layer is CuO and the bottom half is Cu_2O, considering that the oxidation temperature used in this paper is 250 °C. This assumption is consistent with the work done by Haugsrud,[29] in which he proposed that the CuO layer was around 70% of the total oxide thickness if the copper was oxidized at 500 °C. In addition, Hauffe pointed out that the CuO layer thickness decreased with the decrease of oxidation temperature.[18] The assumed distribution of CuO and Cu_2O in the thickness direction is integrated into the two-dimensional (2D) laser ablative cleaning model.

B. Single-pulse irradiation strategy

Under the single-pulse irradiation strategy, the aim is to remove the oxide layer as completely as possible in a single pulse without damaging the substrate.

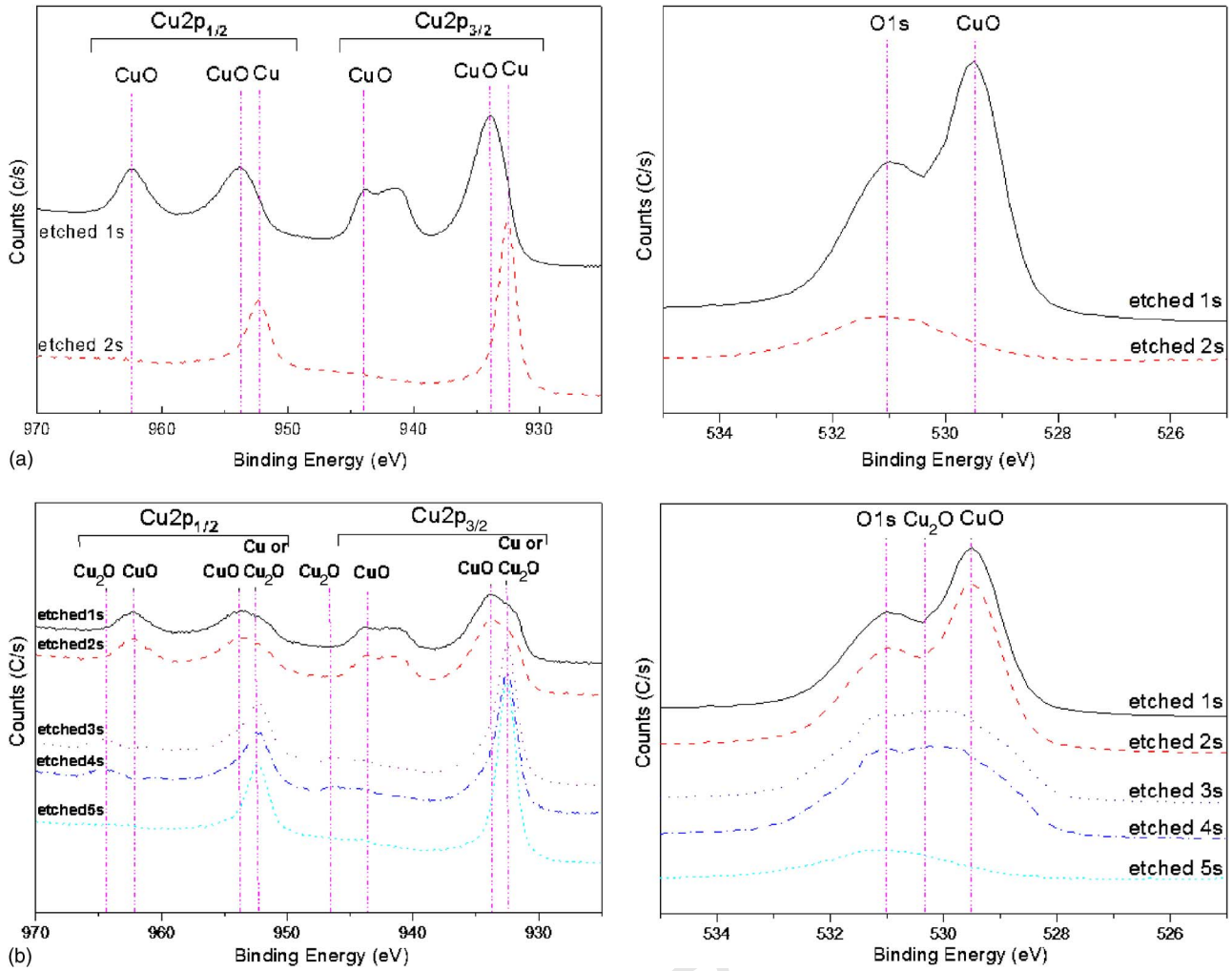

FIG. 4. (Color online) XPS spectra of etched copper samples with copper oxide layers: (a) sample 1 (oxidized at 250 °C for 30 min) and (b) sample 2 (oxidized at 250 °C for 45 min).

1. Experiment

Figure 5 presents the removal results of copper oxide layers with different laser intensity levels. For the sample with the 1 μm thick copper oxide, the intensity of 2.5×10^7 W/cm^2 makes the oxide film rip off without melting. This is possibly due to the shock wave generated by the quick thermal expansion of the material induced by the laser pulse. When the intensity rises to 3.7×10^7 W/cm^2, the copper oxide begins to melt. If the intensity reaches 8×10^7 W/cm^2, the substrate of the copper begins to melt. The laser intensity threshold is defined as the intensity with which a single pulse can remove the oxide layer as completely as possible without any damage to the substrate. Accordingly, the laser intensity threshold is determined as 7.5×10^7 W/cm^2. For the sample with the 2.5 μm thick copper oxide, the similar results are obtained with the corresponding intensity threshold of 2×10^8 W/cm^2. It is clearly shown in Fig. 5 that the laser intensity threshold increases with the thickness of oxide layer.

TABLE I. XPS data for copper oxides.

		Binding energy (eV)	
XPS Cu $2p_{3/2}$	932.4(Cu)	932.4(Cu_2O)	934.5(CuO)
XPS Cu $2p_{1/2}$	952.2(Cu)	952.2(Cu_2O)	954.3(CuO)
XPS O 1*s*	531 (O)	530.3(Cu_2O)	529.5(CuO)

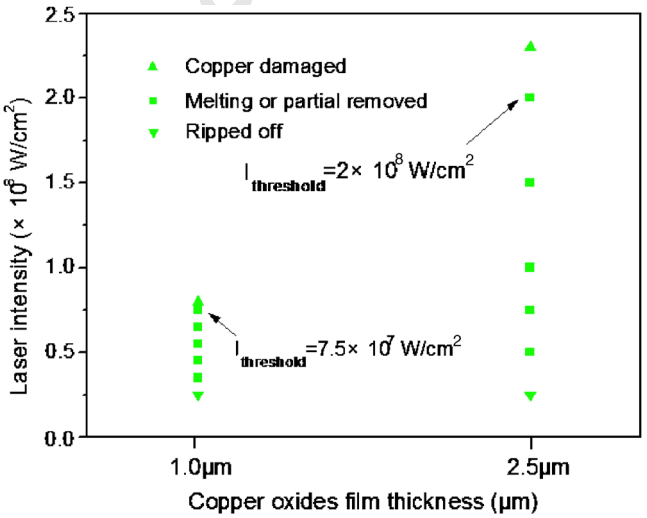

FIG. 5. (Color online) Effects of laser intensity on the removal of copper oxide layers having different thicknesses (beam radius: 20 μm, pulse duration: 50 ns, and pulse number: 1).

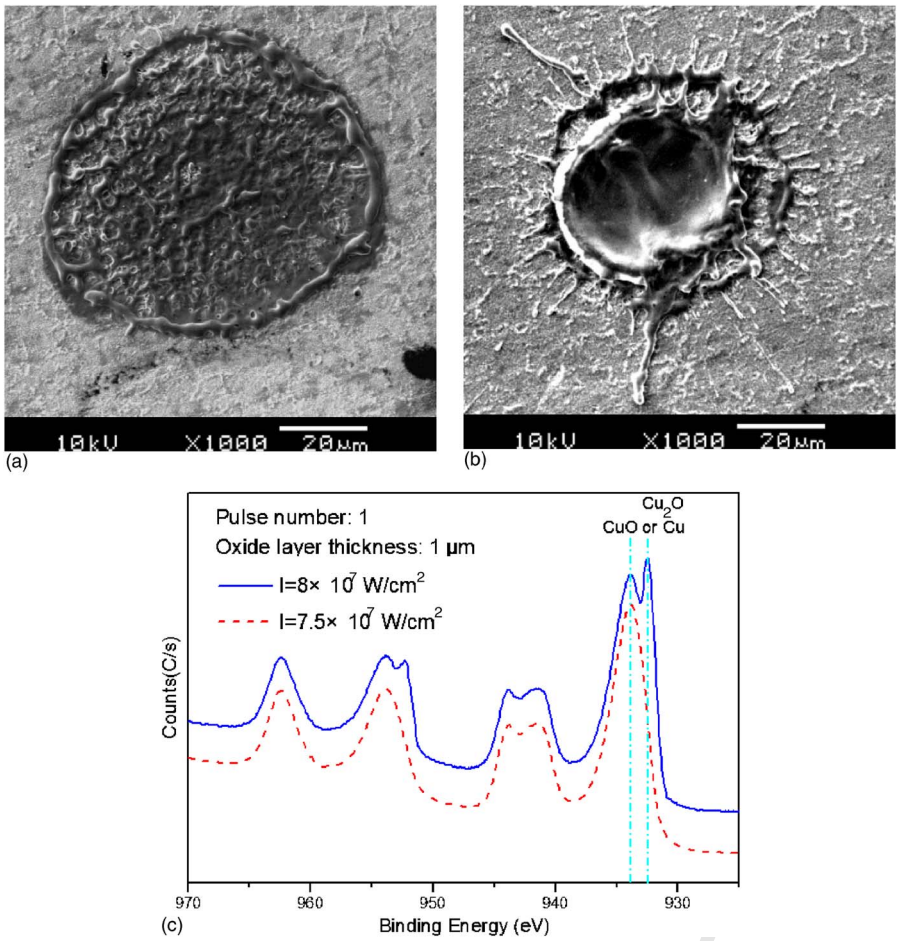

FIG. 6. (Color online) SEM images of the copper oxide layers irradiated by a single pulse with different laser intensities and the corresponding XPS spectra: (a) laser intensity=7.5 $\times 10^7$ W/cm^2, (b) laser intensity=8 $\times 10^7$ W/cm^2, and (c) XPS spectrum (beam radius: 20 μm, pulse duration: 50 ns, oxide layer thickness: 1 μm, and pulse number: 1).

The SEM images shown in Fig. 6 are those of the surface of the sample with the 1 μm thick copper oxide irradiated by two laser intensity levels. It can be seen that the copper oxide is not totally removed by one pulse with the intensity of 7.5×10^7 W/cm^2. However, a little higher intensity leads to a damage in the substrate. This indicates that it is difficult to experimentally determine a safe laser intensity threshold under this strategy.

XPS spectra shown in Fig. 6(c) are aimed at further confirming the cleaning results shown in Figs. 6(a) and 6(b). The sample is irradiated by a matrix of 4×15 spots with the spacing of 200 μm to improve the quality of the XPS signal since the detected area of XPS is around 1 mm^2. For 7.5 $\times 10^7$ W/cm^2, the Cu $2p_{3/2}$ main peak is at 934.5 eV, corresponding to CuO. And the satellite line of CuO also appears. This means that the pulse at this intensity threshold does not remove the copper oxide completely and does not damage the copper substrate. For 8×10^7 W/cm^2, the XPS spectrum has a Cu $2p_{3/2}$ peak at 932.4 eV with a shoulder at 934.5 eV, which corresponds to Cu and/or Cu_2O and CuO. Cu is determined because the satellites of Cu_2O do not exist. All of the satellite lines are related to CuO. Evidently, the copper substrate is exposed due to the removal of the copper oxide.

2. Model prediction and comparison

The experimentally determined intensity thresholds are applied into the two-dimensional laser ablative cleaning model. The experimental and simulated results of crater depths and widths are listed in Table II. The simulation slightly overestimates the ablation effects perhaps due to the insufficient consideration about plasma absorption of laser intensity and the neglect of the heat loss at the surface in the two-dimensional cleaning model. The overestimation is beneficial to a safe cleaning.

TABLE II. Experimental and simulated craters generated by the experimentally determined laser intensity threshold.

Oxide layer thickness (μm)	Intensity threshold (W/cm^2)	Crater depth (μm)		Crater width (μm)	
		Experimental	Simulated	Experimental	Simulated
1	7.5×10^7	0.954±0.1	1.04	45±1.2	48
2.5	2×10^8	2.48±0.15	2.58	53±2	60

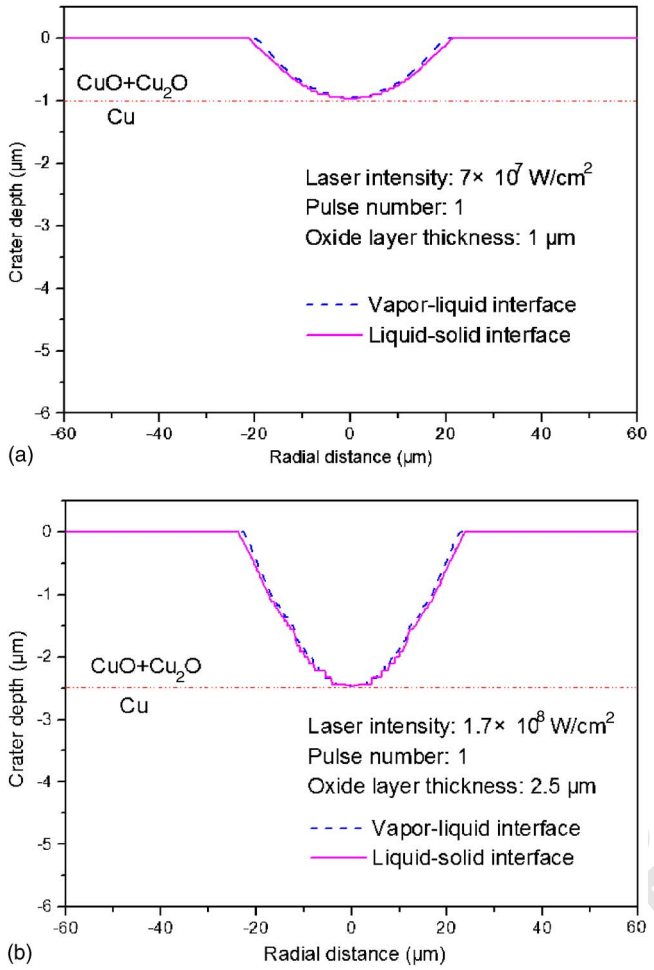

FIG. 7. (Color online) Numerical simulation of craters generated by the single pulse with the model-determined intensity threshold corresponding to the different oxide layer thicknesses: (a) oxide layer thickness=1 μm and intensity threshold=7.5×10^7 W/cm^2 and (b) oxide layer thickness =2.5 μm and intensity threshold=1.7×10^8 W/cm^2 (beam size: 20 μm, pulse duration: 50 ns, and pulse number: 1).

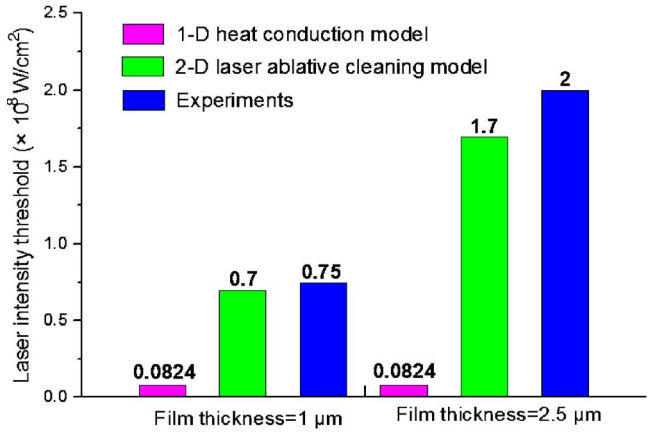

FIG. 8. (Color online) Comparison of laser intensity thresholds determined by the one-dimensional (1D) heat conduction model, the 2D laser ablative cleaning model, and the experiments for the removal of copper oxide layers having different thicknesses (beam radius: 20 μm, pulse duration: 50 ns, and pulse number: 1).

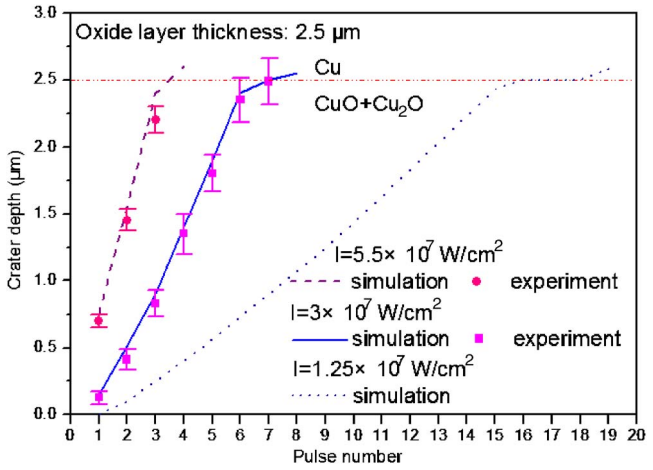

FIG. 9. (Color online) Experiments and simulations of the crater depth increase with the pulse number under two laser intensity levels (beam radius: 35 μm, pulse duration: 50 ns, oxide layer thickness: 2.5 μm and repetition rate=1 kHz).

On determining the intensity threshold with the two-dimensional laser ablative cleaning model, the intensity which makes the temperature of the Cu surface 30 K below 1356 K (Cu's melting point) at the end of the laser pulse is regarded as the intensity threshold. According to this criterion, the intensity threshold is determined as 7×10^7 and 1.7×10^8 W/cm^2 for samples with 1 and 2.5 μm thick oxide layers, respectively. Obviously, the thresholds determined by this model again slightly overestimate experimental results for the reason stated above. Figure 7 shows the craters generated by laser intensity thresholds determined by the two-dimensional cleaning model. There is a thin layer of copper oxide left on the copper surface in both cases.

The one-dimensional heat conduction in a semi-infinite solid model is traditionally used to model the laser ablative removal of oxides. The temperature at the surface is given by $T(0,t)=2I(1-\mathrm{Rl})/K(\sqrt{\alpha t/\pi})$, where I is the laser intensity, Rl is the surface reflectivity, K is the heat conductivity, and α is the heat diffusivity. Suppose that the laser intensity heating the surface to the evaporation temperature at the end of the pulse (50 ns in this case) is the intensity threshold. Therefore, the CuO evaporation threshold of 8.24×10^6 W/cm^2 is regarded as the cleaning threshold.

The thresholds determined by the experiments, the one-dimensional heat conduction model, and the two-dimensional laser ablative cleaning model are shown in Fig. 8. The one-dimensional model determined threshold is far below the experimentally determined thresholds, and is unrelated to the oxide layer thickness. The thresholds determined by the two-dimensional model are very close to the experimental values. Clearly, this two-dimensional laser ablative cleaning model can more accurately estimate the threshold.

C. Multiple-pulse irradiation strategy

Using multiple pulses with a lower intensity is an alternative to the single-pulse mode in that it offers an easier control over the avoidance of damage to the substrate. But it takes a longer time, and pulse repetition rate plays a role.

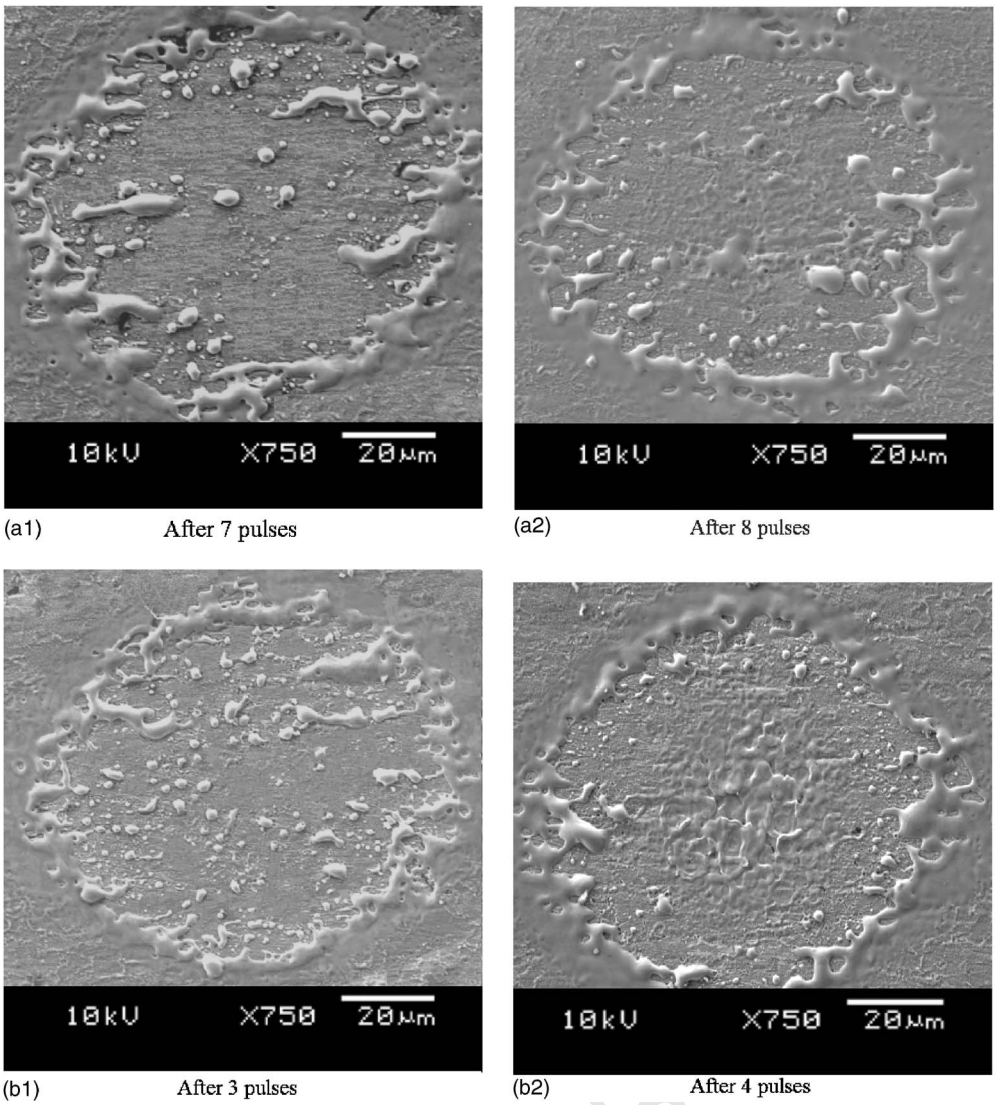

FIG. 10. SEM images of samples cleaned by multiple pulses having different laser intensities: (a) laser intensity $=3\times10^7$ W/cm^2 and (b) laser intensity $=5.5\times10^7$ W/cm^2 (beam radius: 35 μm, pulse duration: 50 ns, oxide layer thickness: 2.5 μm, and repetition rate=1 kHz).

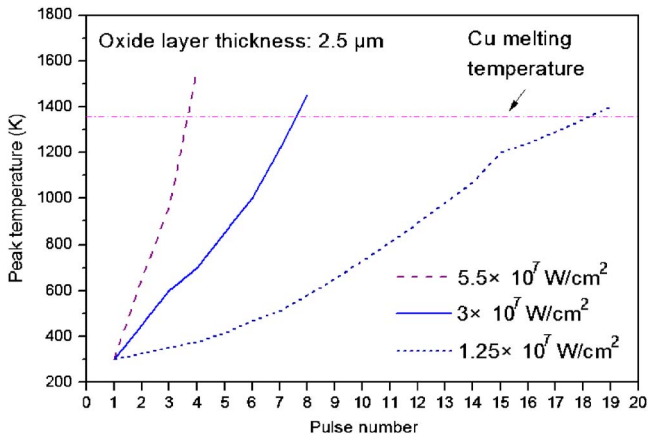

FIG. 11. (Color online) Simulation of peak temperature at the location corresponding to the beam center on the copper surface induced by different pulse numbers with different laser intensities (beam radius: 35 μm, pulse duration: 50 ns, oxide layer thickness: 2.5 μm, and repetition rate=1 kHz).

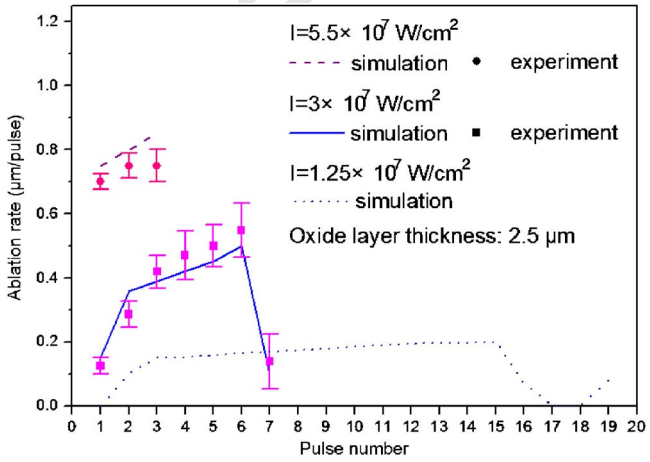

FIG. 12. (Color online) Experiments and simulations of the ablation rate produced by different pulse numbers with different laser intensities (beam radius: 35 μm, pulse duration: 50 ns, oxide layer thickness: 2.5 μm, and repetition rate=1 kHz).

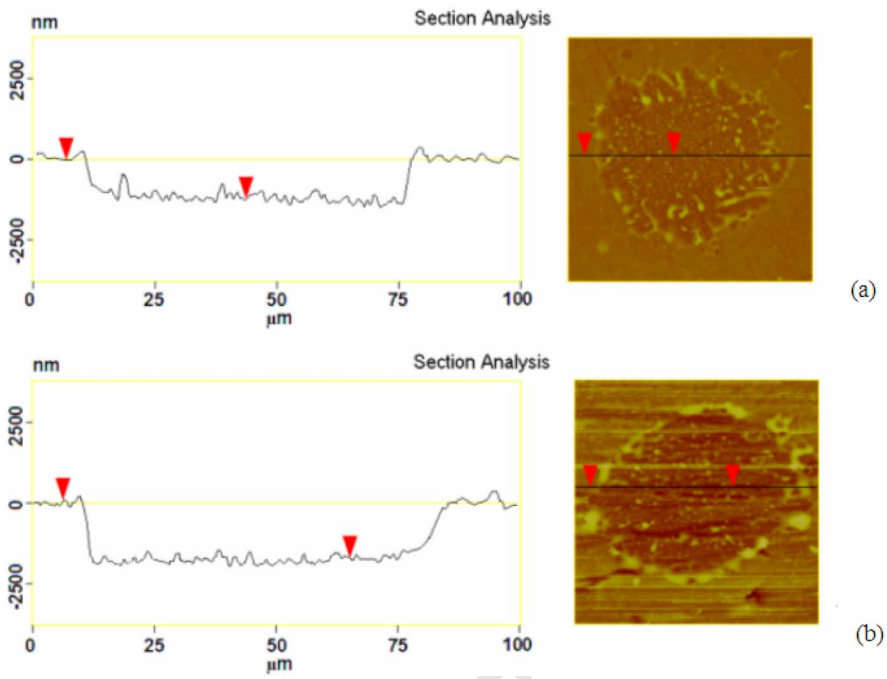

FIG. 13. (Color online) AFM measurements of the craters generated by four laser pulses with different repetition rates: (a) 1 kHz and (b) 2 kHz (laser intensity: 3×10^7 W/cm^2, beam radius: 35 μm, pulse duration: 50 ns, and oxide layer thickness: 2.5 μm).

1. Effect of laser intensity

The laser intensity under the multiple-pulse strategy should be higher than the evaporation threshold of CuO and lower than the melting threshold of the Cu substrate. The former is determined at 1.19×10^7 W/cm^2 by the two-dimensional laser ablative cleaning model, and the latter is determined at 6.5×10^7 W/cm^2 by the two-dimensional laser ablation model in Ref. 19. Hence, three laser intensity values of 1.25×10^7, 3.0×10^7, and 5.5×10^7 W/cm^2 are chosen for the following investigation.

Figure 9 shows the experimental and simulated results of the variation of the crater depth with the pulse number under different laser intensity levels. The experimental crater depth was measured using AFM. Please note that there are no experimental results of the crater depth when the substrate is damaged. This is because the damaged substrate becomes so rough at the local area that AFM cannot be used. In addition, for the intensity of 1.25×10^7 W/cm^2, only simulation results are shown.

With the intensity of 5.5×10^7 W/cm^2, three pulses cannot completely remove the oxide film, and four pulses do damage the substrate. For the intensity of 3×10^7 W/cm^2, the crater produced by the seventh pulse ceases to deepen after the very thin oxide layer left by the sixth pulse is removed, and the eighth pulse makes the Cu surface start to melt. SEM images of the sample surfaces corresponding to the above mentioned four cases are shown in Fig. 10. The surface morphology is consistent with the results shown in Fig. 9. With the intensity of 1.25×10^7 W/cm^2, the oxide layer is completely removed after the irradiation of 15 pulses. However, the 16th, 17th, and 18th pulses directly irradiating the naked Cu substrate show no damage to the Cu surface.

Figure 11 shows the simulated peak temperature induced by different pulse numbers at the point on the copper substrate corresponding to the beam center. With the intensity of 1.25×10^7 W/cm^2, the peak temperature induced by 16, 17, and 18 pulses is below 1356 K, which confirms the existence of an intact copper surface. It can be concluded that the excessive number of pulses with this rather low laser intensity will not damage the copper substrate. On the other hand, the peak temperature corresponding to the case of the Cu surface melting goes beyond 1356 K, namely, four pulses with the intensity of 5.5×10^7 W/cm^2 and eigth pulses with the intensity of 3×10^7 W/cm^2.

The ablation rate is defined as the thickness of the oxide layer removed by a pulse, equal to the depth of the crater generated by a pulse. Figure 12 shows the experimental and simulated ablation rates with different pulse numbers under two intensity levels. The ablation rate increases with the increase in laser intensity, which agrees with the fact that less pulse numbers are required under higher laser intensities shown in Fig. 9. In addition, with the identical laser intensity, the ablation rate also increases with the pulse number. This is due to the continuous increase of heat accumulation with the pulse number. However, for the intensity of 3×10^7 W/cm^2, the ablation rate of the seventh pulse becomes smaller since this intensity is not sufficiently high to damage the Cu substrate.

Most simulated ablation rates are higher than the corresponding experimental values due to the overestimation of temperature in the simulation. However, the experimental ablation rates of the third to the sixth pulse with the intensity of 3×10^7 W/cm^2 are higher than the simulated values, possibly due to the involvement of the shock wave. The shock wave induced by the plasma gets stronger with the increase in pulse number.

2. Effect of repetition rate

Figure 13 shows the AFM measured craters produced by four pulses with the intensity of 3×10^7 W/cm^2 under the repetition rates of 1 and 2 kHz, respectively. It is observed

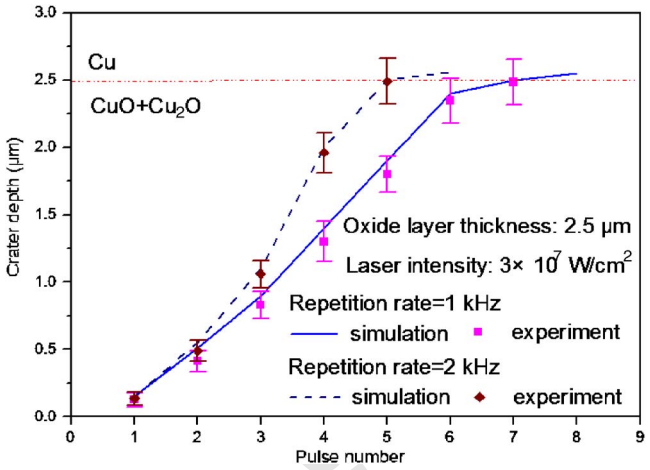

FIG. 14. (Color online) Experiments and simulations of the crater depth increase with the pulse number under two laser repetition rates (laser intensity: 3×10^7 W/cm^2, beam radius: 35 μm, pulse duration: 50 ns, and oxide layer thickness: 2.5 μm).

that the crater produced under 1 kHz is shallower and narrower than that under 2 kHz. The experimental and simulated results on the variation of the crater depth with the pulse number under different repetition rates are presented in Fig. 14. The depth of the crater after five pulses under 2 kHz is roughly equal to that after seven pulses produced under 1 kHz. Obviously, the lower pulse number is required in the case of the high repetition rate. Figure 15 shows the simulated crater generated by five pulses with the laser intensity of 3×10^7 W/cm^2 under the repetition rates of 1 and 2 kHz and the corresponding temperature distribution in the material. The simulated variation of the crater depth with the repetition rate is very similar to the experimentally obtained one shown in Fig. 13.

Figure 16 shows the simulated temperature history of the point on the Cu surface corresponding to the beam center. The pulse periods corresponding to the repetion rates of 1 and 2 kHz are 1 and 0.5 ms, respectively. With the pulse period decreasing, the heat dissipating time between two consecutive laser pulses gets shorter and the temperature decreases less. Thus, more heat is accumulated. This fact can be seen in Fig. 16. Due to the more severe heat accumulation in the case of 2 kHz, the temperature induced by the fifth pulse is significantly higher than that under 1 kHz. This is the reason that higher repetition rates can reduce the required pulse number to remove the oxide layer under the identical laser intensity.

Figure 16 also shows that the temperature rise induced by one pulse gets larger with the pulse number. This is be-

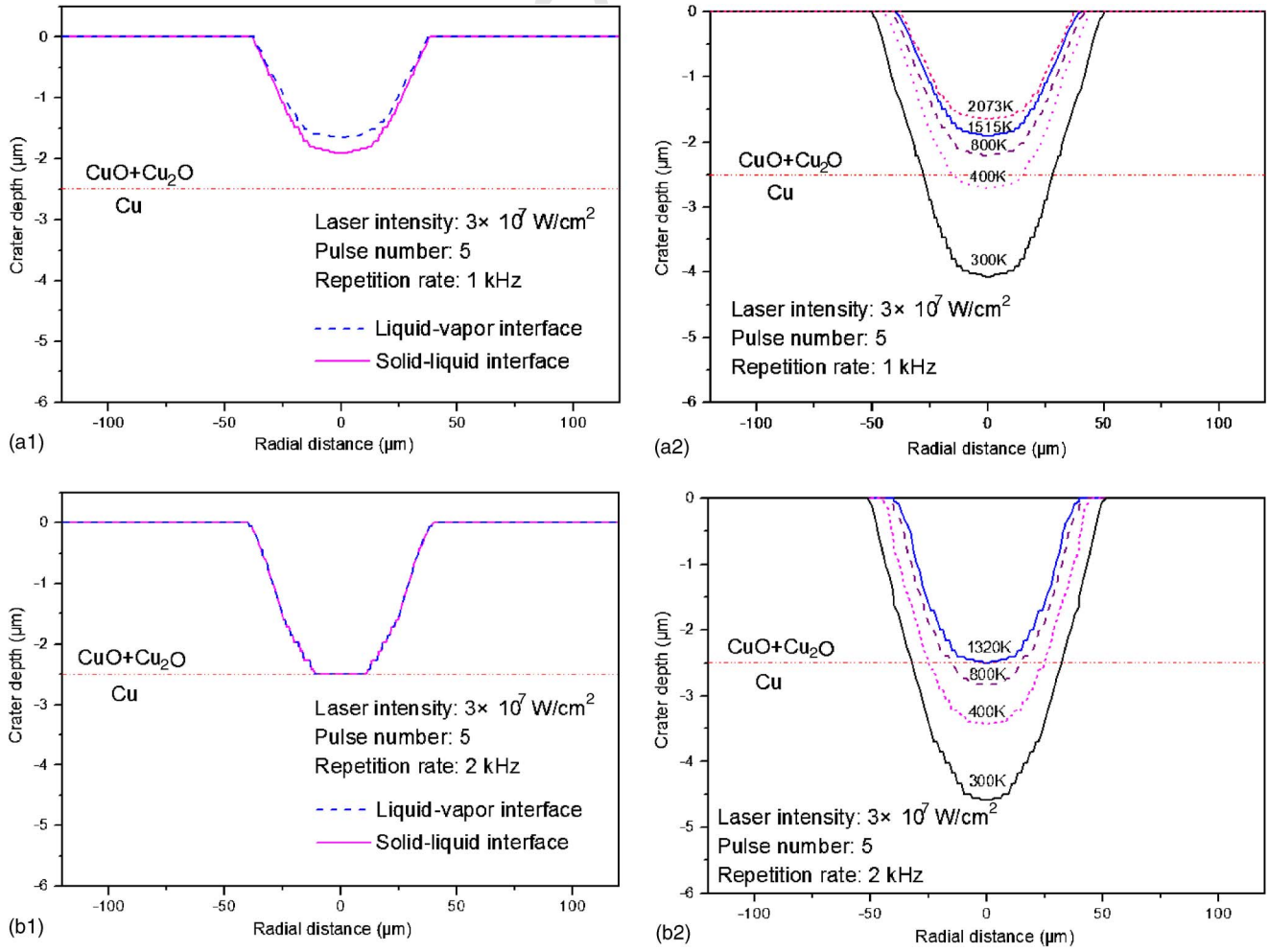

FIG. 15. (Color online) Simulations of craters generated by five pulses and the corresponding isothermal contours in the material: (a) 1 kHz and (b) 2 kHz (laser intensity: 3×10^7 W/cm^2, beam radius: 35 μm, pulse duration: 50 ns, and oxide layer thickness: 2.5 μm).

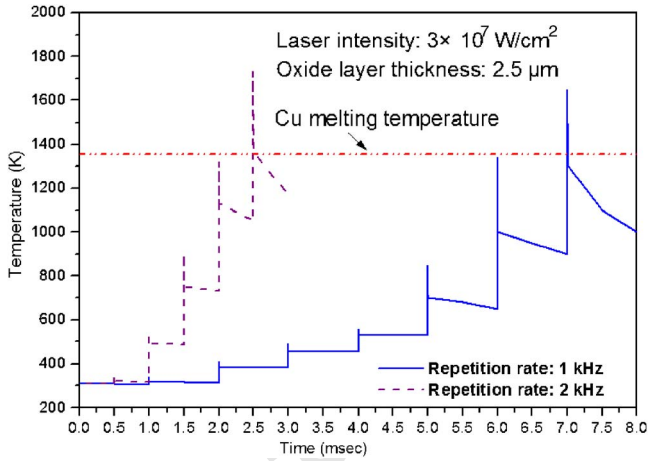

FIG. 16. (Color online) Simulated time history of temperature at the location corresponding to the beam center on the Cu surface during the irradiation of pulses with different repetition rates (laser intensity: 3×10^7 W/cm^2, beam radius: 35 μm, pulse duration: 50 ns, and oxide layer thickness: 2.5 μm).

cause the laser irradiation approaches the Cu surface more and more as the above copper oxide layer is continuously ablated by the successive laser pulses. Thus, the temperature on the Cu surface increases more by the same energy with the pulse number.

V. CONCLUSIONS

Different oxide layer thicknesses with CuO and Cu_2O distributions in the thickness direction are considered. The two-dimensional laser ablative cleaning model has a two-layer structure and is used to comparatively study single-pulse and multiple-pulse irradiation strategies. Under the single-pulse strategy, the cleaning process can be completed with a single pulse, but the intensity threshold that does not cause substrate damage is difficult to experimentally determine. This model can determine the intensity threshold with a safety margin not to damage the underlying substrate. Under the multiple-pulse strategy, it takes multiple pulses to remove an oxide layer without damaging the substrate, while the laser intensity has a much larger window of operation. With a little lower laser intensity, it takes more pulses to remove the oxide, but a few extra pulses will not damage the substrate and will thus give a larger safety margin. The higher the laser repetition rate, the lower the laser pulse number that is required for safe cleaning.

ACKNOWLEDGMENTS

The authors are grateful to Adrian M. Chitu, Alex Wu, and Shengguo Jia for their technical assistance during the AFM, XPS, and ellipsometer measurements, respectively.

[1]W. Zapka, W. Ziemlich, and A. C. Tam, Appl. Phys. Lett. **58**, 2217 (1991).
[2]X. Zhou, K. Imasaki, H. Furukawa, H. Umino, K. Sakagishi, S. Nakai, and C. Yamanaka, Surf. Eng. **17**, 384 (2001).
[3]A. C. Tam, W. P. Leung, W. Zapka, and W. Ziemlih, J. Appl. Phys. **71**, 3515 (1992).
[4]A. Tsunemi, K. Hagiwara, N. Saito, K. Nagasaka, Y. Miyamoto, O. Suto, and H. Tashiro, Appl. Phys. A: Mater. Sci. Process. **A63**, 435 (1996).
[5]P. Meja, M. Autrie, P. Alloncle, P. Pasquet, R. Oltra, and J. P. Boquillon, Appl. Phys. A: Mater. Sci. Process. **A69**, 687 (1999).
[6]J. Solis, F. Vega, and C. N. Afonso, Appl. Phys. A: Mater. Sci. Process. **A62**, 197 (1996).
[7]H. Lim and D. Kim, J. Laser Appl. **16**, 25 (2004).
[8]W. M. Steen, Laser Material Processing (Springer-Verlandag, London, 1998).
[9]J. Magyar, A. Sklyarov, K. Mikaylichenko, and V. Yakovlev, Appl. Surf. Sci. **207**, 306 (2003).
[10]P. Psyllaki and R. Oltra, Mater. Sci. Eng., A **282**, 145 (2000).
[11]D. A. Wesner, M. Mertin, F. Lupp, and E. W. Kreutz, Appl. Surf. Sci. **96–98**, 479 (1996).
[12]Y. Yonezawa, T. Minamikawa, A. Morimoto, and T. Shimizu, Jpn. J. Appl. Phys., Part 1 **37**, 4505 (1998).
[13]A. Kearns, C. Fischer, K. G. Watkins, M. Glasmacher, H. Kheyrandish, A. Brown, W. M. Steen, and P. Beahan, Appl. Surf. Sci. **127–129**, 773 (1998).
[14]J. M. Lee, K. G. Watkins, and W. M. Steen, ASME J. Manuf. Sci. Eng. **23**, 521 (2001).
[15]S. K. Lee, K. K. Yoon, K. H. Whang, and S. J. Na, Surf. Coat. Technol. **113**, 63 (1999).
[16]R. M. A. Azzam and N. M. Bashara, *Ellipsometry and Polarized Light* (North-Holland, New York, 1977).
[17]J. C. Vickerman, *Surface Analysis: The Principal Techniques* (Wiley, Chichester, England, 1997).
[18]K. Hauffe, *Oxidation of Metals* (Plenum, New York, 1965).
[19]W. W. Zhang, Y. L. Yao, and K. Chen, Int. J. Adv. Manuf. Technol. **18**, 323 (2001).
[20]G. V. Samsonov, *The Oxide Handbook* (IFI/Plenum, New York, 1982).
[21]I. S. Grivoriev and E. Z. Meilikhov, *Handbook of Physical Quantities* (CRC, New York, 1997).
[22]W. Duley, *UV Lasers: Effects and Applications in Materials Science* (Cambridge University Press, Cambridge, 1996).
[23]E. Palik, *Handbook of Optical Constants of Solids II* (Academic, San Diego, 1991).
[24]A. M. Meirmanov, *The Stefan Problem* (Walter de Gruyter, Berlin, 1992).
[25]C. J. Knight, AIAA J. **17**, 519 (1979).
[26]V. R. Voller and C. Prakash, Int. J. Heat Mass Transfer **30**, 140 (1987).
[27]S. V. Patankar, *Numerical Heat Transfer and Fluid Flow* (Hemisphere, Roman, 1990).
[28]J. Chastain and J. R. King, *Handbook of X-ray Photoelectron Spectroscopy* (Physical Electronics, Eden Prairie, 1995).
[29]R. Haugsrud, J. Electrochem. Soc. **149**, B14 (2002).